J. Membrane Biol. 170, 213–227 (1999)

The Journal of
Membrane
Biology



# Rectification of the Olfactory Cyclic Nucleotide-Gated Channel by Intracellular Polyamines

**J.W. Lynch**
Department of Physiology and Pharmacology, University of Queensland, Brisbane, QLD 4072, Australia

Received: 17 February 1999/Revised: 27 April 1999

**Abstract.** Polyamine-induced inward rectification of cyclic nucleotide-gated channels was studied in inside-out patches from rat olfactory neurons. The polyamines, spermine, spermidine and putrescine, induced an 'instantaneous' voltage-dependent inhibition with $K_d$ values at 0 mV of 39, 121 μM and 2.7 mM, respectively. Hill coefficients for inhibition were significantly < 1, suggesting an allosteric inhibitory mechanism. The Woodhull model for voltage-dependent block predicted that all 3 polyamines bound to a site ⅓ of the electrical distance through the membrane from the internal side. Instantaneous inhibition was relieved at positive potentials, implying significant polyamine permeation. Spermine also induced exponential current relaxations to a 'steady-state' impermeant level. This inhibition was also mediated by a binding site ⅓ of the electrical distance through the pore, but with a $K_d$ of 2.6 mM. Spermine inhibition was explained by postulating two spermine binding sites at a similar depth. Occupation of the first site occurs rapidly and with high affinity, but once a spermine molecule has bound, it inhibits spermine occupation of the second binding site via electrostatic repulsion. This repulsion is overcome at higher membrane potentials, but results in a lower apparent binding affinity for the second spermine molecule. The on-rate constant for the second spermine binding saturated at a low rate (~200 $sec^{-1}$ at +120 mV), providing further evidence for an allosteric mechanism. Polyamine-induced inward rectification was significant at physiological concentrations.

**Key words:** Spermine — Spermidine — Putrescine — Woodhull — Block

*Correspondence to:* J.W. Lynch

## Introduction

The detection of odorants by olfactory receptor neurons is mediated by odorant-sensitive G protein-coupled receptors. When stimulated, these receptors induce a rapid increase in cAMP, which in turn directly activates the olfactory-specific cylic nucleotide-gated (CNG) cation channel. When activated, these channels initiate neuronal depolarization and mediate a calcium influx (Frings et al., 1995). Calcium influx then activates a chloride-selective channel, which greatly amplifies the transduction signal (Kurahashi & Yau, 1993; Lowe & Gold, 1993). Thus, CNG channels form a crucial link between the stimulus-induced chemical change and the electrical signal that is transmitted to higher brain centers. Calcium influx through CNG channels is also important for signal desensitization (Kurahashi & Shibuya, 1990). In general, the physiological role of any ion channel is strongly dependent on factors which govern its conductance-voltage relationship (Hille, 1992). It is already known that physiological concentrations of external $Ca^{2+}$ and $Mg^{2+}$ and internal $Mg^{2+}$ are able to exert strong voltage-dependent block of olfactory CNG channels (Zufall & Firestein, 1993; Lynch & Lindemann, 1994). However, other factors may also be responsible for controlling the voltage-dependence of these channels *in vivo*.

The naturally occurring polyamines, spermine, spermidine and putrescine, were recently shown to be responsible for inward rectification in the strong inward rectifier $K^+$ ($K_{ir}$) channel family (Fakler et al., 1994, 1995; Ficker et al., 1994; Lopatin, Makhina & Nichols, 1994). These molecules have since been shown to induce inward rectification in a variety of other cation-selective ion channel types (reviewed in Williams, 1997), including the recombinantly expressed rod CNG α subunit (Lu & Ding, 1999). Polyamines appear to bind in the pore of ion channels and exert their effects by

either direct channel block or by modulating intrinsic gating activity. Investigation of the mechanisms of action of polyamines has enhanced our understanding not only of physiological ion channel regulatory mechanisms, but also of the molecular structure and function of ion channel pores (reviewed in Nichols & Lopatin, 1997; Williams, 1997).

Polyamines are essential for protein synthesis and cell growth and are present in virtually all cell types (Tabor & Tabor, 1984). It may be expected that they would be particularly important in olfactory receptor neurons, which regenerate continually throughout life. However, the roles of polyamines on olfactory receptor neuronal development or physiological function have not been investigated. In particular, the possibility that physiological concentrations of polyamines may regulate the activity of the olfactory CNG channel has not previously been studied. This report provides evidence that physiological concentrations of spermine and spermidine do, in fact, confer strong inward rectification on rat olfactory CNG channels.

## Materials and Methods

Olfactory receptor neurons were isolated from adult rats as previously described (Lynch & Barry, 1991). Dissociated cells were continuously superfused by a modified Tyrode's solution containing (in mM): NaCl 140, KCl 5, $CaCl_2$ 2, $MgCl_2$ 1, glucose 10, and HEPES 10 (pH 7.4 with NaOH). Membrane currents were recorded using standard patch-clamp techniques. Patch pipettes, fabricated from borosilicate haematocrit tubing, had tip resistances of between 8–12 MΩ when filled with the standard divalent cation-free pipette solution containing (in mM): NaCl 140, EGTA 10, HEPES 10, (pH 7.4 with NaOH). Olfactory receptor neurons were readily identified by their distinct bipolar shape. Cell-attached membrane patches were formed among the cilia on the apical knobs of these cells and detached into the inside-out configuration by exposure to fast flowing control solution. Solutions were applied by a multi-barrel perfusion system as described previously (Balasubramanian, Lynch & Barry, 1995).

Excised patches were exposed to a low divalent cation solution containing (in mM): NaCl 140, EDTA 0.25, HEPES 10 (pH 7.4 with NaOH). Unless otherwise indicated, this was the standard control solution used in all experimental procedures. Both cAMP and the polyamines, spermine, spermidine and putrescine, were dissolved directly into this solution. Excised patches were voltage-clamped at 0 mV and macroscopic patch currents were measured in response a standard voltage-clamp protocol. This consisted of a 20 msec preconditioning step to −120 mV to remove any time-dependent block that may have accumulated at the holding potential of 0 mV. This was immediately followed by a depolarizing step of 120 msec duration to voltages from −120 to +120 mV in 20 mV steps (*see* Fig. 1*A*, inset). Currents were recorded using an Axopatch 1D patch-clamp amplifier (Axon Instruments, Foster City, CA). Except where indicated, data were filtered at 2 kHz by the internal amplifier filter and digitized at 5 kHz directly onto an IBM Pentium PC. A Digidata 1200 interface controlled by Pclamp6 software (Axon Instruments) was used to control patch pipette potential and data acquisition parameters. Polyamines and cAMP were obtained from Sigma (St. Louis, MI) or ICN Biomedicals (Aurora, OH). All experiments were performed at room temperature.

The cAMP-activated currents used for analysis and display were obtained by digitally subtracting currents recorded in the absence of cAMP from those recorded in its presence. Current traces were not averaged. Sigmaplot 3.0 (Jandel, San Rafael, CA) was used to fit data by a least-squares fitting routine. All averaged experimental results are expressed as mean ± one SEM. Statistical significance was assessed using either a paired or unpaired *t*-test, as appropriate, with a $P$ value of $< 0.05$ being considered significant.

## Results

### Spermine Block

The effects of spermine on the rat olfactory cyclic nucleotide-gated channel were investigated in inside-out patches excised from the dendritic knob of dissociated rat olfactory receptor neurons. Such patches frequently contain several hundred active CNG channels. An example of macroscopic currents activated by a saturating (20 μM) concentration of cAMP in one patch is shown in Fig. 1*A* (top left panel). Membrane patches were sequentially exposed to spermine at concentrations of 10, 30, 100, 300 and 1,000 μM. Examples of currents recorded at 0, 10, 100 and 1,000 μM spermine are displayed in Fig. 1*A*. It is apparent from this figure that there is both an instantaneous and a time-dependent decrease in current. Current-voltage relationships for both

**Fig. 1.** The effects of intracellular spermine on the olfactory CNG channel. (*A*) CNG currents recorded from a single inside-out patch in response to the application of a saturating (20 μM) concentration of cAMP together with indicated concentrations of spermine. The 'control' current traces (top left) were recorded in the absence of spermine. The voltage-clamp protocol is explained in the text and is illustrated in the inset. The asterisk indicates an example of a spermine-induced local minimum in the channel conductance near 0 mV. (*B*) Current-voltage relationships for the peak and steady-state currents displayed in (*A*). In both panels, control currents are indicated by filled circles, and 10, 100 and 1000 μM spermine are represented by unfilled circles, filled triangles and unfilled triangles, respectively. Peak currents (left panel) were measured as the maximal current magnitude reached immediately upon step depolarization to each test potential. Steady-state currents (right panel) were averaged over the final 40 msec of each 120 msec depolarization to each test potential. (*C*) Sampling rate does not affect peak current magnitude. Both panels show currents activated by 20 μM cAMP both in the absence (small dots) and presence (large dots) of 1 mM spermine. In the left panel, the data were filtered at 2 kHz and digitized at 5 kHz. In the right panel, the data were filtered at 20 kHz and digitized at 50 kHz. All traces were recorded in successive sweeps from the same patch. In both the left and right panels, the peak current ratios were 0.20 and 0.19, respectively. Similar experiments were performed in a total of 3 patches, where the mean low and high resolution peak current ratios were 0.18 ± 0.04 and 0.21 ± 0.05, respectively. Using a paired *t*-test, these results are not significantly different.

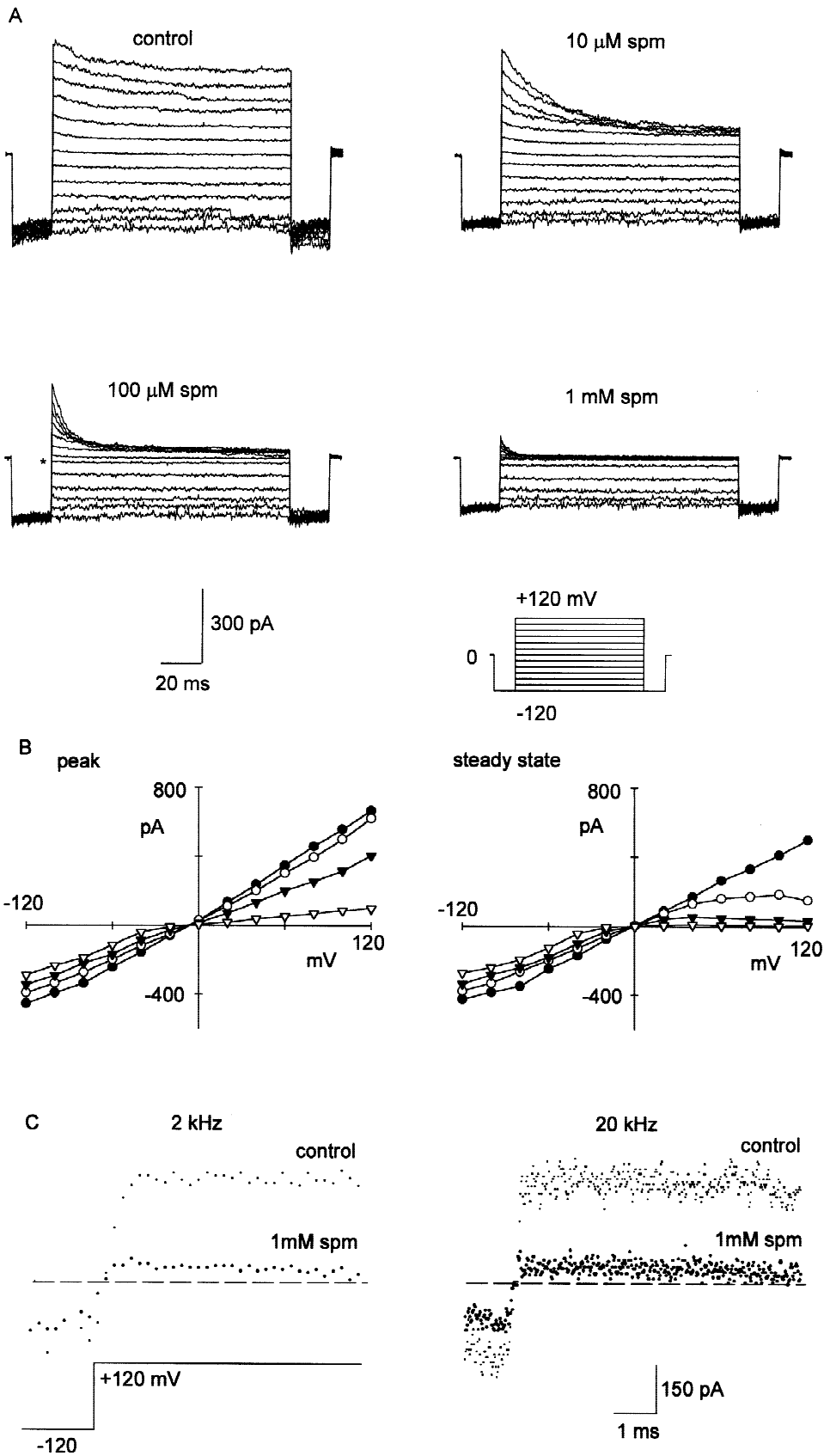
A
control
10 μM spm
100 μM spm
1 mM spm
300 pA
20 ms
+120 mV
0
-120
B
peak
steady state
800
pA
-120
120
mV
-400
C
2 kHz
20 kHz
control
1mM spm
+120 mV
-120
150 pA
1 ms

**Fig. 1.**

peak and steady-state currents in Fig. 1*A* are displayed in Fig. 1*B*. Peak currents were measured as the average of the first 3 digitized points recorded following the completion of the depolarizing step to each potential. Steady-state currents were averaged over all points in the final 40 msec at each depolarizing step.

It was necessary to establish that the filtering and digitization rates (2 and 5 kHz, respectively) were sufficient to completely resolve peak current magnitudes. As seen in Fig. 1*A*, the most rapid current transients occurred following patch depolarization to +120 mV in the presence of 1 mM spermine. Fig. 1*C* shows cAMP-gated currents recorded upon depolarization from −120 to +120 mV both in the absence (small dots) and presence (large dots) of 1 mM spermine. In the left panel, currents were filtered at 2 kHz and digitized at 5 kHz, and in the right panel, currents from a different sweep in the same patch were filtered at 20 kHz and digitized at 50 kHz. As discussed in the legend to Fig. 1*C*, filtering at 2 kHz did not significantly attenuate current peak magnitudes.

An unusual feature of spermine block is that both the steady-state and peak conductances reached a local minimum near 0 mV. This is particularly apparent in the current traces corresponding to 100 μM spermine (Fig. 1*A*, asterisk). The spermine-induced inhibition was quantitated by plotting the ratios of peak and steady-state conductances recorded at each concentration of spermine relative to those measured in the absence of spermine. In Fig. 2*A*, the peak conductance ratios averaged from 5 patches are shown as filled circles, and the steady-state conductance ratios averaged from the same 5 patches are shown as unfilled circles. This figure reveals several features of spermine-induced inhibition. At negative membrane potentials, there is no time-dependent inhibition and hence the steady-state and instantaneous conductance ratios overlap. The degree of spermine inhibition increases with depolarization and reaches a local minimum near 0 mV. At spermine concentrations >10 μM, the instantaneous conductance then shows a tendency to increase from −10 to +50 mV, whereupon it remains approximately constant up to +120 mV. In contrast, the steady-state inhibition shows a pronounced voltage- and concentration-dependent inhibition at voltages > +10 mV. For each spermine concentration and membrane potential, the steady-state conductance is plotted as a ratio of peak conductance in Fig. 2*B*. This figure shows that the steady-state level of inhibition is attaiend in a voltage- and concentration-dependent manner from the instantaneous level of inhibition.

In $K_{ir}2.1$, membrane hyperpolarization results in a slow rate of spermine unblock (Lopatin, Makhina & Nichols, 1995). However, in the olfactory CNG channel, recovery from block at negative membrane potentials was too fast to resolve. This is suggested in Fig. 1*A*, where the magnitude and the activation time courses of the currents at −120 mV appear to be independent of the previous patch potential. This was confirmed by depolarizing membrane patches to +120 mV for 20 msec to effect complete steady-state block, then stepping down to membrane potentials of +100 to −120 mV in 20 mV steps. In each of 3 patches subjected to this voltage-clamp protocol, the recovery from steady-state block displayed no time-dependence at any membrane potential.

Since the voltage- and concentration-dependence of instantaneous and steady-state block are different (Fig. 2A and *B*), it is possible that their respective effects are mediated by distinct spermine binding sites. This possibility was investigated by fitting the instantaneous and steady-state conductance data with the Woodhull (1973) model which is often used to describe voltage-dependent ion channel block. The model can be represented by the Boltzmann-type equation:

$$K_d = K_{d(0)} \cdot \exp(-z\delta V_m F/RT) \quad (1)$$

where $K_d$ is the spermine dissociation constant, $V_m$ is the membrane potential, $K_{d(0)}$ is the dissociation constant at 0 mV, $z$ is the valence of the blocker, δ is the fraction of the membrane electric field from the intracellular side that affects the binding interaction, and $F$, $R$ and $T$ are the Faraday constant, the ideal gas constant and the absolute temperature, respectively. In the original form of the Woodhull equation, the $K_d$ values were calculated using the expression:

$$G/G_{max} = 1/(1 + [p]/K_d) \quad (2)$$

where $G/G_{max}$ is the ratio of the blocked to unblocked conductance and $[p]$ is the polyamine concentration. The instantaneous conductance data from Fig. 2*A* (filled circles) were replotted as a function of spermine concentration in Fig. 3*A*. For clarity, only instantaneous $G/G_{max}$ values corresponding to membrane potentials from −70 to −10 mV are shown. The solid lines in Fig. 3*A* show that Eq. 2 does not provide a good fit to the data. The steady-state $G/G_{max}$ values from Fig. 2*C* were replotted as a function of spermine concentration in Fig. 3*C*. Again, the solid lines demonstrate that Eq. 2 does not provide an adequate description of steady-state block. Thus, spermine block of the olfactory CNG channel is not well described by the original Woodhull equation.

The spermine inhibitory dose-responses were then fitted to the following equation:

$$G/G_{max} = 1/(1 + [p]^h/K_d{}^h) \quad (3)$$

where $h$ is the Hill coefficient. As shown by the lines of best fit in Fig. 3*B* and *D*, this equation more accurately modelled the spermine-induced amplitude reductions at

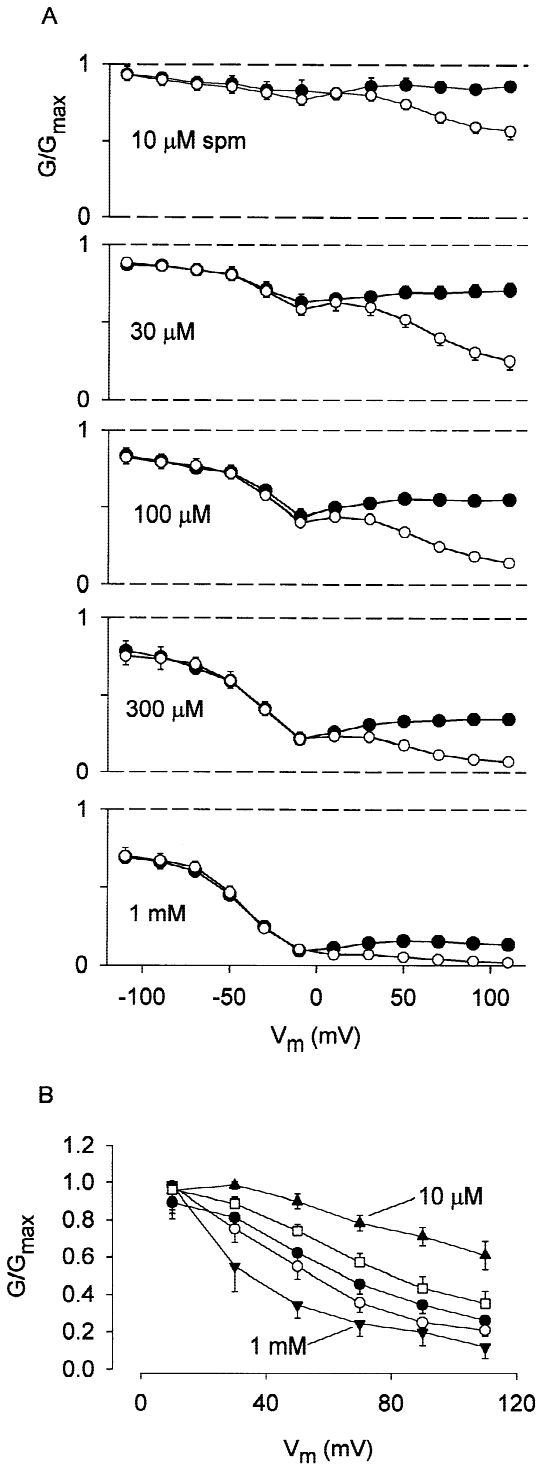


**Fig. 2.** Conductance-voltage relationships for spermine instantaneous and steady-state block. (*A*) The spermine instantaneous conductance ratio (filled circles) was calculated as the ratio of the peak conductance in the presence of spermine ($G$), relative to the peak conductance in the absence of spermine ($G_{max}$), at each membrane potential. Similarly, the steady-state block conductance ratio (unfilled circles) was calculated as the ratio of steady-state conductance in the presence of spermine, relative to the steady-state conductance in the absence of spermine. In this analysis, the conductance ($G$ or $G_{max}$) at any membrane potential $X$ mV, was calculated as the mean of the currents ($I$ or $I_{max}$) recorded at $X - 10$ mV and $X + 10$ mV. It was necessary to define $G/G_{max}$ in this manner to avoid the large errors that result when calculating direct current ratios (i.e., $I/I_{max}$) at voltages close to the reversal potential. All displayed points represent averaged data from 5 patches. In this and all subsequent figures, error bars (± SEM) are displayed when larger than symbol size. (*B*) Ratios of steady-state to peak $G/G_{max}$ values for the data displayed in (*A*). The points represent spermine concentrations of 10 μM (filled triangles), 30 μM (unfilled squares), 100 μM (filled circles), 300 μM (unfilled circles) and 1 μM (filled inverted triangles).

all membrane potentials. The averaged $K_d$ values for instantaneous and steady-state spermine block from 5 patches each fitted using Eq. 3 are shown in Fig. 3*E* as filled and unfilled circles, respectively. The corresponding Hill coefficients for instantaneous and steady-state block are shown in Fig. 3*F* as filled and unfilled circles, respectively. It is apparent in Fig. 3*E* that the $K_d$ values for instantaneous block (filled circles) decrease as a monotonic function of membrane potential between −110 and −10 mV. However, at more positive voltages they display a slight increase. As discussed below, this later effect may be due to a combination of incomplete block at saturating spermine concentrations and spermine permeation. Inspection of the fitted curves in Fig. 3*B* suggests that the instantaneous spermine inhibitory dose-responses became progressively steeper between −70 and −10 mV. The Hill coefficients did, in fact, display a significant increase over this voltage range (Fig. 3*F*, filled circles). Using a paired *t*-test to compare the $h$ values at −10 mV with those at −70 mV, revealed a statistically significant increase ($P = 0.016$). However, at more depolarized membrane potentials, the Hill coefficient for instantaneous block remained constant near 0.75. A possible explanation for the low value and voltage-dependence of $h$ is considered below. The steady-state $K_d$ values for spermine block also displayed a monotonic decrease with voltage between +30 and +120 mV (Fig. 3*E*, unfilled circles), while their respective mean Hill coefficients remained constant near 0.5 at all voltages examined (Fig. 3*F*, unfilled circles).

Linear regression of $K_d$ between −110 and −10 mV gave a mean $z\delta$ for instantaneous block of 1.27 ± 0.13 ($n = 5$) and a mean extrapolated $K_{d(0)}$ of 39 ± 7 μM ($n = 5$). Assuming that all 4 spermine charges contribute to the binding reaction, this analysis estimates δ as 0.32 ± 0.03. A similar analysis revealed that the steady-state inhibition had a mean $z\delta$ of 1.18 ± 0.06 ($n = 5$) and a $K_{d(0)}$ of 2.6 ± 0.7 mM ($n = 5$). Using an unpaired *t*-test, the respective $z\delta$ values for instantaneous and steady-state block are not significantly different ($P = 0.55$). Thus, the binding sites for both fast and slow spermine block are located at an identical depth in the pore.

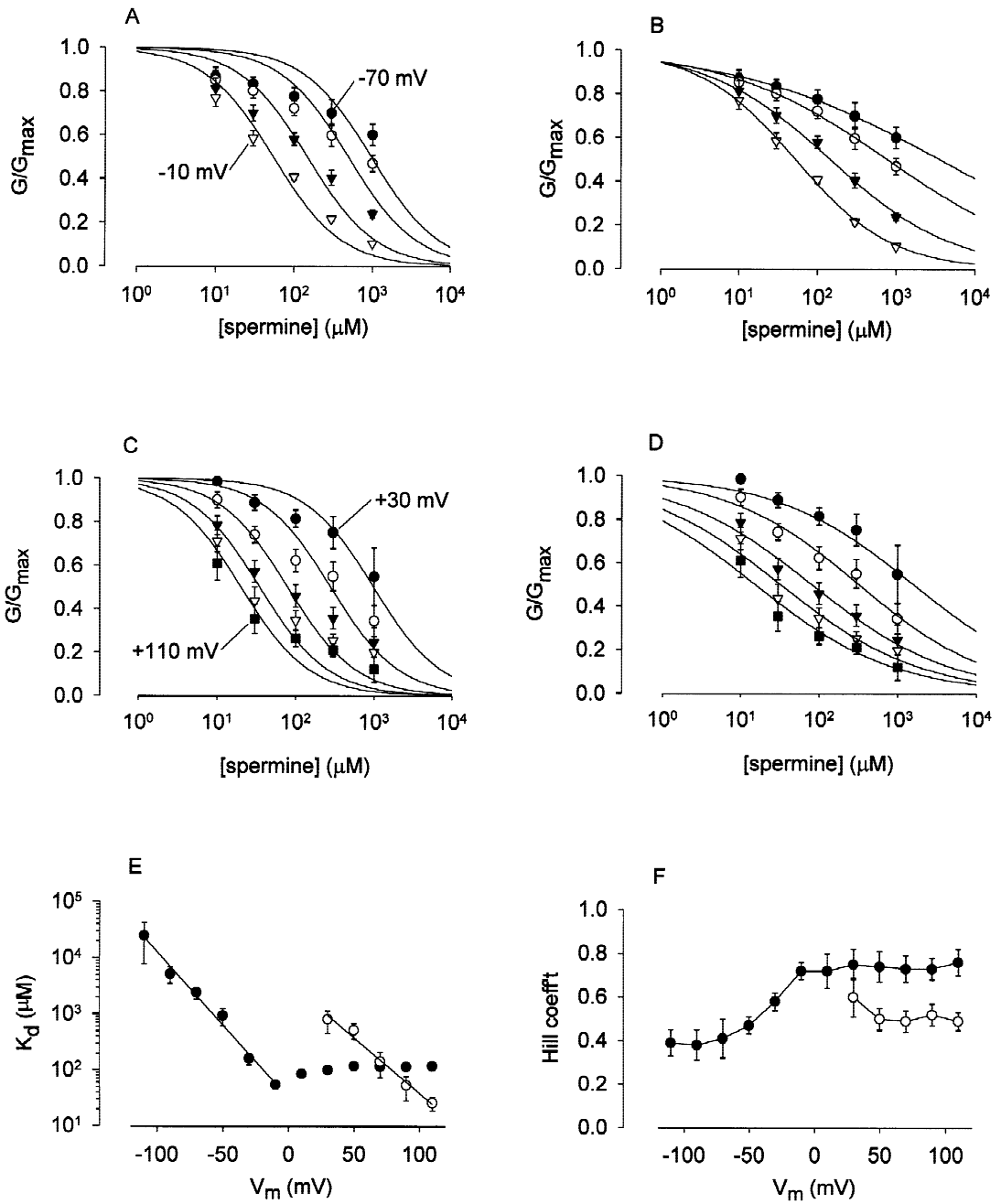


**Fig. 3.** Determination of mean $K_d$ and $h$ for instantaneous and steady-state spermine block. (*A*) Instantaneous $G/G_{max}$ values at membrane potentials from −70 to −10 mV plotted as a function of spermine concentration. Points correspond to membrane potentials of −70 mV (filled circles), −50 mV (unfilled circles), −30 mV (filled inverted triangles) and −10 mV (unfilled inverted triangles). Points are replotted from data displayed in Fig. 2*A*. Curves represent the best fits of Eq. 2. The $K_d$ values of best fit were: 965 μM (−70 mV), 490 μM (−50 mV), 147 μM (−30 mV) and 54 μM (−10 mV). (*B*) Data points replotted from (*A*) fitted by Eq. 3. The displayed curves were generated using the following values of best fit for $K_d$ and $h$, respectively: 3567 μM, 0.34 (−0.70 mV); 776 μM, 0.43 (−50 mV); 148 μM, 0.57 (−30 mV); and 53 μM, 0.72 (−10 mV). (*C*) Steady-state $G/G_{max}$ values at membrane potentials from +30 to +120 mV plotted as a function of spermine concentration. Points correspond to membrane potentials of +30 mV (filled circles), +50 mV (unfilled circles), +70 mV (filled inverted triangles), +90 mV (unfilled inverted triangles) and +110 mV (filled squares). Points are replotted from data displayed in Fig. 2*B*. Curves represent the best fits of Eq. 2, with $K_d$ values of best fit as follows: 986 μM (+30 mV), 279 μM (+50 mV), 79 μM (+70 mV), 35 μM (+90 mV) and 20 μM (+110 mV). (*D*) Data points replotted from (*C*) fitted by Eq. 3 with the following values of best fit for $K_d$ and $h$, respectively: 1469 μM, 0.60 (+30 mV); 324 μM, 0.52 (+50 mV); 81 μM, 0.48 (+70 mV); 33 μM, 0.49 (+90 mV); and 16 μM, 0.52 (+110 mV). (*E*) $K_d$ values of best fit using Eq. 3 for instantaneous $G/G_{max}$ values (filled circles) and steady-state $G/G_{max}$ values (unfilled circles). Regression lines are fitted to all steady-state $G/G_{max}$ values and to instantaneous $G/G_{max}$ values between −110 and −10 mV. (*F*) Hill coefficient values of best fit using Eq. 3 for instantaneous $G/G_{max}$ values (filled circles) and steady-state $G/G_{max}$ values (unfilled circles).

### Analysis of the Time Dependence of Spermine Block

Analysis of the time dependence of the development of steady-state block should reveal estimates of the association and dissociation rate constants for the steady-state binding reaction. The current relaxations observed at membrane potentials ≥ +60 mV were fitted with the exponential function:

$$I(t) = A \cdot \exp(t/\tau) + B \quad (4)$$

where $A$ and $B$ are the amplitudes of the instantaneous and steady-state currents, respectively, $t$ is time and $\tau$ is the decay time constant. Estimates for $A$, $B$ and $\tau$ were obtained by fitting currents with a nonlinear least squares curve-fitting routine. Examples of curve fits to Eq. 4 for currents from one patch exposed to 300 μM spermine are displayed in Fig. 4*A*. A similar analysis was performed on currents corresponding to spermine concentration of 30–1,000 μM in each of 4 patches and the averaged $\tau$ values are presented in Fig. 4*B*. In all patches, the current decay rates were well approximated by a single exponential term, implying that steady-state inhibition can be approximated as a simple bimolecular reaction. Hence, the block and unblock rate constants can be calculated using the following equations:

$$k_b = (1 - I_{ss}/I_{peak})/\tau \quad (5)$$

and

$$k_u = (I_{ss}/I_{peak})/\tau \quad (6)$$

where $k_b$ and $k_u$ are the block and unblock rate constants, respectively, and $I_{ss}/I_{peak} = B/(A + B)$. The averaged block and unblock rate constants, plotted as a function of spermine concentration, are shown in Fig. 5*A*. The unblock rates were not affected by changes in either voltage or spermine concentration (Fig. 5*A*, lower panel) and hence were extrapolated to 0 mV and averaged for all spermine concentrations to yield a mean dissociation rate constant ($K_u$) of 24.4 ± 1.2 $sec^{-1}$ ($n = 4$). In contrast, the $k_b$ was strongly dependent on spermine concentration (Fig. 5*A*, upper panel). As expected for a charged molecule binding to a site within the membrane electrical field, $k_b$ varied as an exponential function of the membrane potential (Fig. 5*B*). This enabled the $k_b$ values at 0 mV to be determined by extrapolation. The mean values for $k_b$ and $k_u$ at 0 mV determined in this manner are shown in Fig. 5*C*. As discussed, the mean $k_b$ values increased linearly with increasing spermine (regression coefft = 0.97). Since the association rate constant ($K_{on}$) for the spermine-receptor interaction at 0 mV is equal to $k_b \cdot$ [spermine], the slope of the $k_b$ regression line ($2.4 \times 10^4 \pm 0.4$ $M^{-1}$ $sec^{-1}$) in Fig. 5*C* provides an estimate for

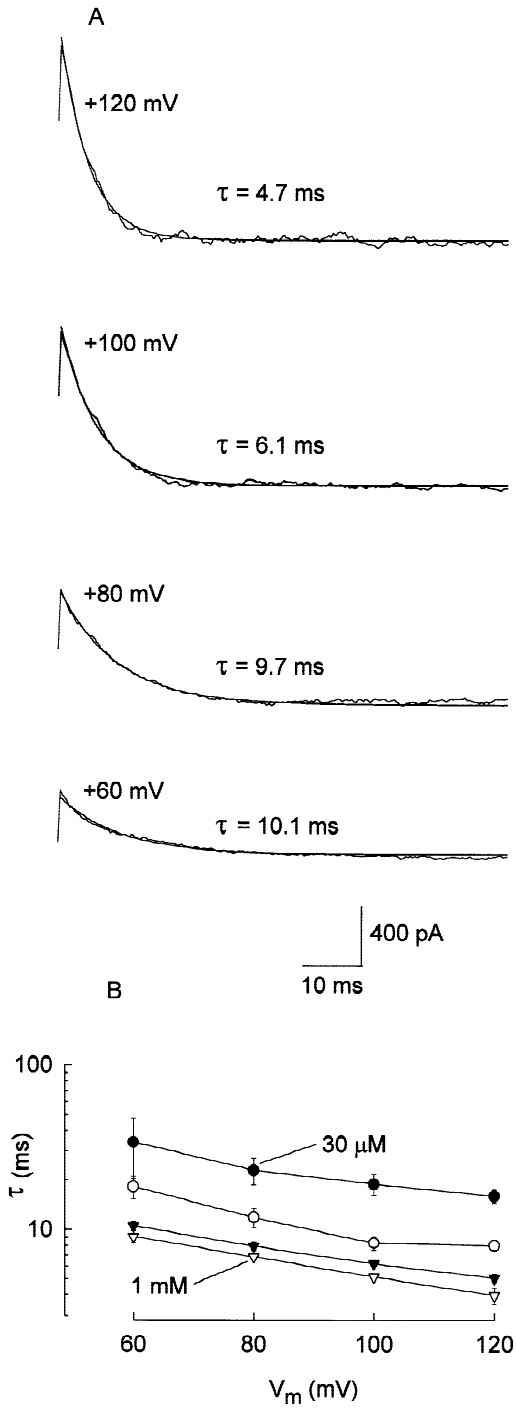


**Fig. 4.** Exponential decay of spermine-induced current relaxations. (*A*) Examples of currents activated by 20 μM cAMP following depolarization from −120 mV to the indicated membrane potentials in the presence of 300 μM spermine. All current traces are from the same patch. Exponential curves of best fit are superimposed on each current trace and their fitted $\tau$ values are indicated. (*B*) Average $\tau$ of best fit for spermine concentrations of 30 μM (filled circles), 100 μM (unfilled circles), 300 μM (filled inverted triangles) and 1 mM (unfilled inverted triangles). All data points are averaged from 4 patches.

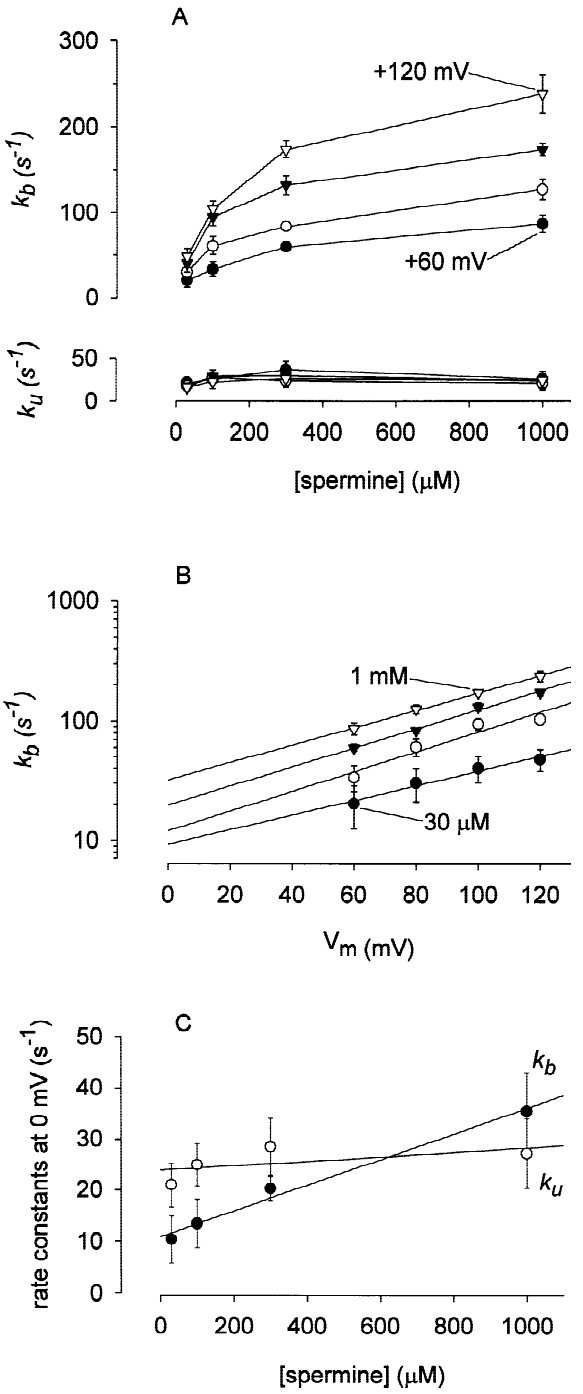


**Fig. 5.** Rate constants for spermine steady-state block. (*A*) Mean blocking ($k_b$) and unblocking ($k_u$) rate constants are plotted for membrane potentials of +60 mV (filled circles), +80 mV (unfilled circles), +100 mV (filled triangles) and +120 mV (unfilled triangles), in the upper and lower panels, respectively. These values were calculated according to Eqs. 5 and 6. (*B*) $k_b$ data points from (*A*) are plotted as a function of membrane potential for spermine concentrations of 30 μM (filled circles), 100 μM (unfilled circles), 300 μM (filled triangles) and 1 mM (unfilled circles). Regression lines, extrapolated to 0 mV, are shown for each concentration. (*C*) Mean block (filled circles) and unblock (unfilled circles) rate constants at 0 mV are plotted as a function of spermine concentration. Smooth lines represent linear regressions. The slope of the $k_b$ regression line is $2.4 \times 10^4 \pm 0.4$ $M^{-1}$ $sec^{-1}$. All data points in this figure are averaged from 4 patches.

$K_{on}$. From the ratio of the rate constants ($K_u/K_{on}$), the equilibrium dissociation constant ($K_{d(0)}$) was estimated as 1.3 ± 0.3 mM ($n = 4$). Using an unpaired *t*-test, this value was not significantly different from that (2.6 ± 0.7 mM) calculated above from the voltage-dependence of steady-state inhibition ($P = 0.17$).

## [cAMP]-Dependence of Spermine Block

Block by spermine was investigated over a range of cAMP concentrations to determine whether it exerted any influence on the apparent binding affinity for cAMP. In this experiment, the inhibitory effect of 300 μM spermine was determined at cAMP concentrations of 2, 5 and 20 μM. These cAMP concentrations represent approximately half-maximal, 75% maximal and saturating concentrations, respectively (Frings, Lynch & Lindemann, 1992). Examples of currents recorded from a single patch in the presence of 2 and 20 μM cAMP, with and without spermine, are displayed in Fig. 6*A*. The time constants for the development of steady-state block were measured at +80, 100 and 120 mV at each [cAMP]. As shown in Fig. 6*B*, results averaged from 3 patches indicate that the decay time constants displayed no significant [cAMP]-dependence. Furthermore, the steady-state $G/G_{max}$ ratios, calculated as described in the legend to Fig. 2, revealed that there was no significant difference in the voltage-dependence of inhibition between 2 and 20 μM cAMP (Fig. 6*C*). Similarly, there was no difference in the voltage-dependence of the peak $G/G_{max}$ ratios (Fig. 6*D*). Together, these results indicate that spermine does not act as a classical competitive antagonist for cAMP. They further indicate that if spermine is acting by interfering with the channel gating mechanism, then its allosteric inhibitory action does not have a reciprocal effect on the cAMP binding affinity (Colquhoun & Farrant, 1993).

## Spermidine and Putrescine Block

The blocking effects of the naturally occurring polyamines, spermidine and putrescine, were also investigated. These molecules contain 3 and 2 positively charged amine groups, respectively. Inhibition by spermidine was investigated at concentrations of 30, 100, 300 and 1,000 μM in the presence of 20 μM cAMP. Examples of the effects of 0, 100 and 1,000 μM spermidine in one patch are shown in Fig. 7*A*. In contrast to the effects of spermine, spermidine caused only instantaneous block, even at strongly depolarized potentials. Spermidine $G/G_{max}$ values averaged from 5 patches are displayed in Fig. 7*B*. As in the case of spermine, the standard Woodhull model (Eq. 2) provided an inadequate fit to the data and this was substantially improved by incorporating a Hill coefficient term as in Eq. 3. The mean $K_d$ and $h$ values for spermidine block derived using Eq. 3 are displayed in Fig. 7*C* and *D*, respectively. As

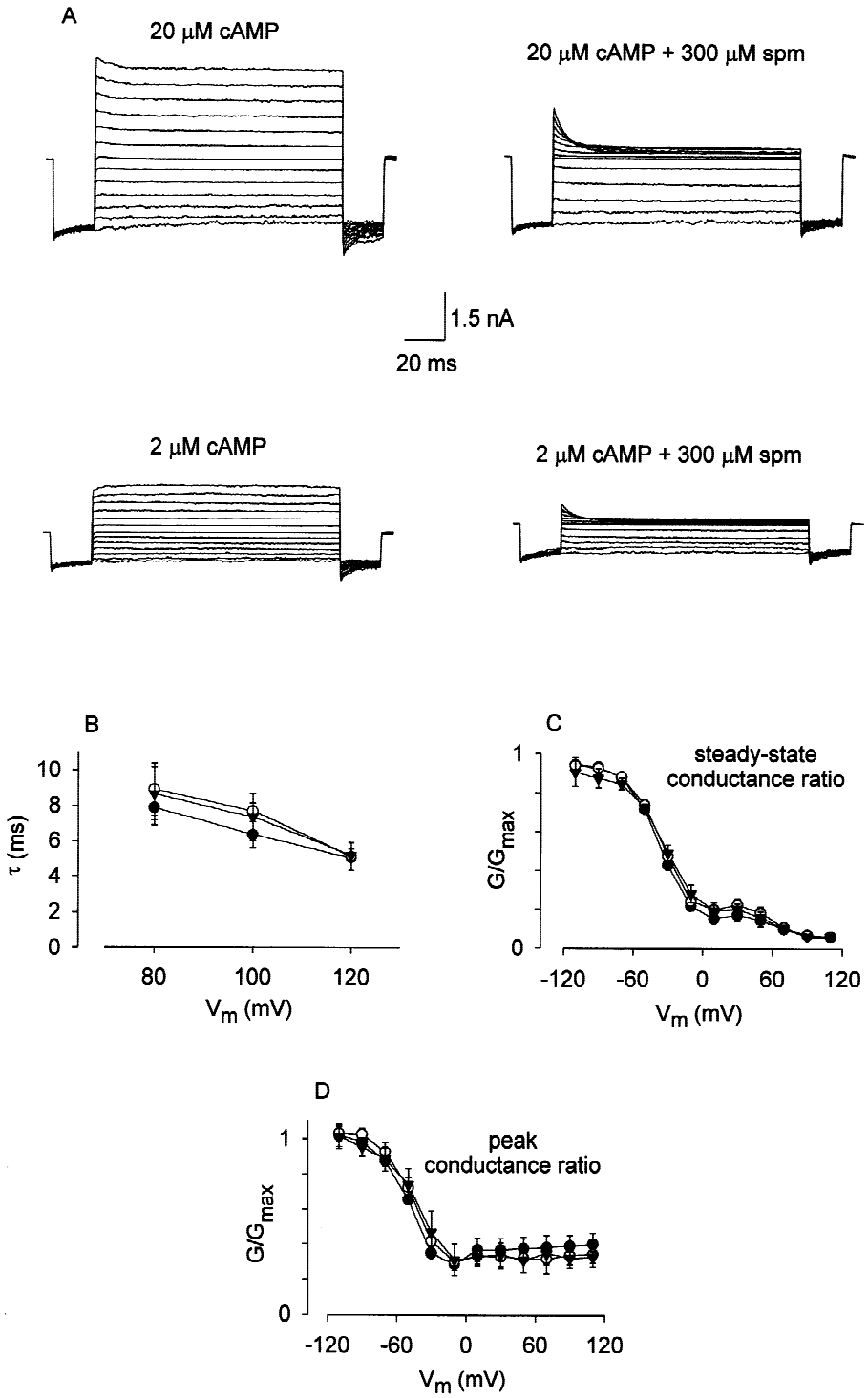


**Fig. 6.** Effect of cAMP concentration on spermine block. (*A*) Examples of currents activated by 20 and 2 μM cAMP are shown in the left hand panel. The effects of 300 μM spermine on currents activated by 20 and 2 μM cAMP are shown in the right hand panel. All currents were recorded from the same patch. (*B*) Mean values of peak to steady-state current decay time constants are plotted for cAMP concentrations of 20 μM (filled circles), 5 μM (unfilled circles) and 2 μM (filled inverted triangles). (*C*) Steady-state $G/G_{max}$ ratios calculated as described in the legend to Fig. 2 for cAMP concentrations of 20 μM (filled circles), 5 μM (unfilled circles) and 2 μM (filled inverted triangles). (*D*) Peak $G/G_{max}$ ratios calculated as described in the legend to Fig. 2 for cAMP concentrations of 20 μM (filled circles), 5 μM (unfilled circles) and 2 μM (filled inverted triangles). All data points in (*B*), (*C*) and (*D*) were averaged from the same 3 patches.

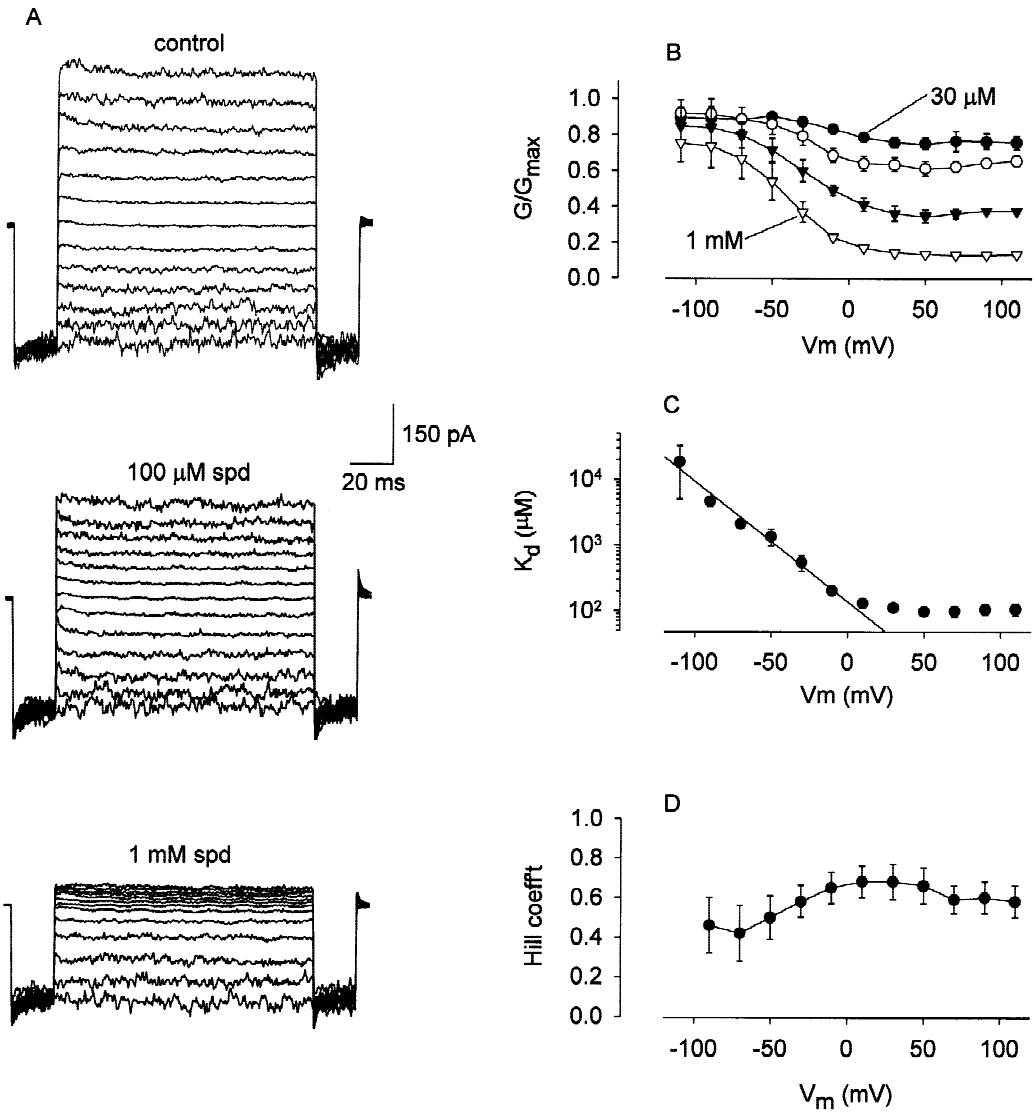


**Fig. 7.** Spermidine block of CNG currents. (*A*) Examples of currents activated by 20 μM cAMP in the presence of 0, 100 μM and 1 mM spermidine. All recordings were from the same patch. (*B*) Average steady-state $G/G_{max}$ ratios, calculated as described in the legend to Fig. 2, for spermidine concentrations of 30 μM (filled circles), 100 μM (unfilled circles), 300 μM (filled inverted triangles) and 1 mM (unfilled inverted triangles). (*C*) Mean $K_d$ values fitted to the data displayed in (*B*) using Eq. 3. A regression line is fitted to points between −110 and −10 mV. (*D*) Mean hill coefficient values fitted to the data in (*B*) using Eq. 3. All data points in (*B*), (*C*) and (*D*) were averaged from 5 patches.

for spermine, the spermidine $K_d$ decreased monotonically from −110 to −10 mV, but at more positive voltages they remained almost constant (Fig. 7*C*). Linear regression of the $K_d$ between −110 and −10 mV yielded a mean $z\delta$ of 1.13 ± 0.06 ($n = 5$) and a $K_{d(0)}$ of 121 ± 16 μM ($n = 5$). Given a valence of 3, the spermidine blocking site occurred at 38 ± 2% of the electrical distance from the internal membrane side. Using an unpaired *t*-test, the difference in the depths of the spermine instantaneous binding site and the spermidine binding site is not statistically significant ($P = 0.20$). Thus, spermine and spermidine bind at a similar depth in the pore. The Hill coefficient values for the spermidine block are displayed in Fig. 7*C*. The maximum mean values were about 0.7. Although a slight voltage-dependent trend is apparent at negative membrane potentials, the difference in the mean *h* values between −50 and −10 mV was not significantly different using a paired *t*-test ($P = 0.27$).

Putrescine block was investigated at concentrations of 0.3, 1, 3 and 10 mM in the presence of 20 μM cAMP. Examples of currents recorded in the presence of 0, 1 and 10 mM putrescine are shown in Fig. 8*A*. As in the case of spermidine, putrescine inhibition also lacked the slowly developing steady-state inhibtion that was observed for spermine at depolarized potentials. Mean $G/G_{max}$ values for putrescine are shown in Fig. 8*B*. The modified ver-

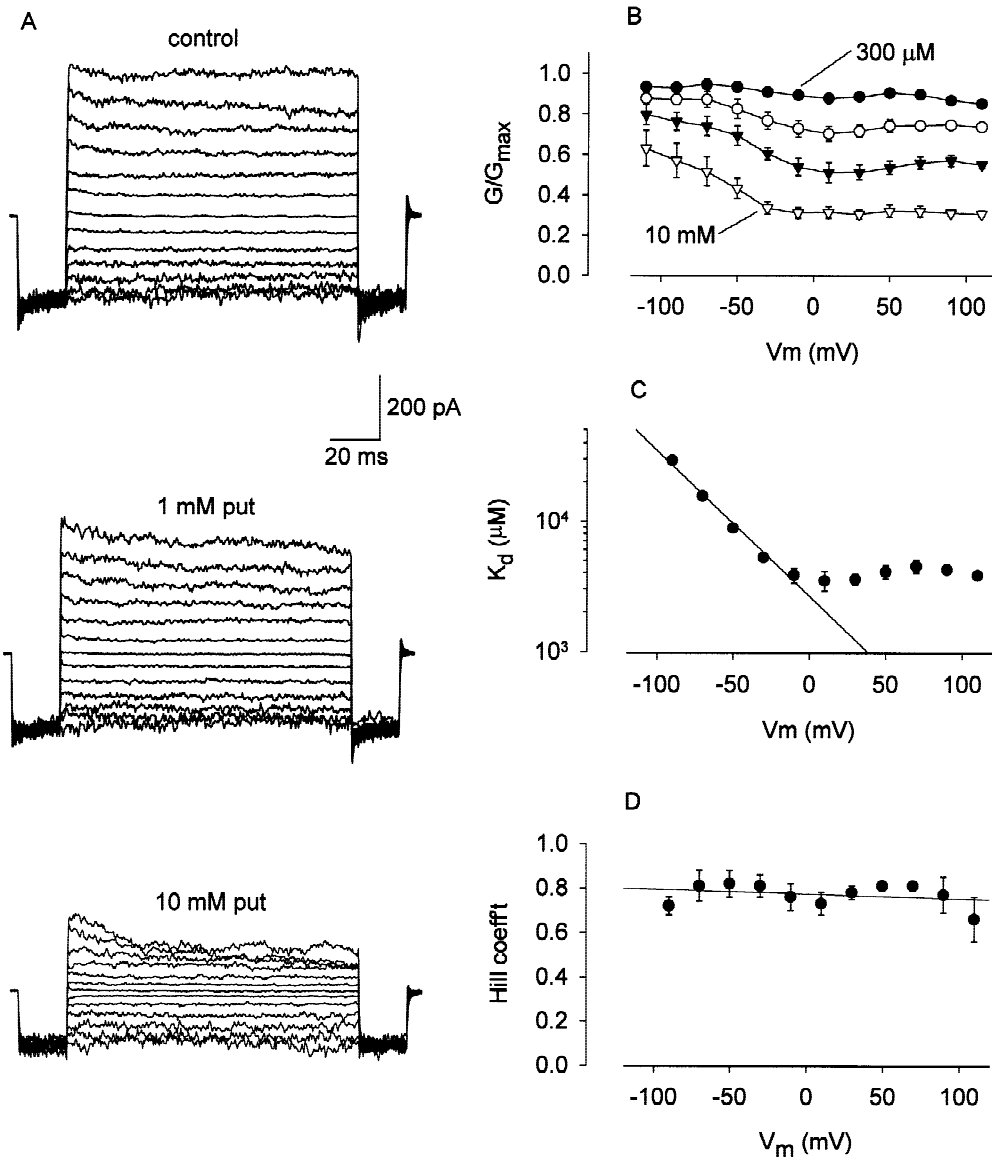


**Fig. 8.** Putrescine block of CNG currents. (*A*) Examples of currents activated by 20 μM cAMP in the presence of 0, 1 and 10 mM putrescine. All recordings were from the same patch. (*B*) Average steady-state $G/G_{max}$ ratios, calculated as described in the legend to Fig. 2, for putrescine concentrations of 300 μM (filled circles), 1 mM (unfilled circles), 3 mM (filled inverted triangles) and 10 mM (unfilled inverted triangles). (*C*) Mean $K_d$ values fitted to the data displayed in (*B*) using Eq. 3. A regression line is fitted to points between −90 and −10 mV. (*D*) Mean hill coefficient values fitted to the data in (*B*) using Eq. 3. The line represents a linear regression through all points. All data points in (*B*), (*C*) and (*D*) were averaged from 3 patches.

sion of the Woodhull equation (Eq. 3) was required to adequately fit the putrescine block data (*not shown*) and yielded mean values for $K_d$ and $h$ as shown in Fig. 8*C* and *D*. Each of these values was averaged from 3 patches. The mean value for $z\delta$, determined by linear regression between −90 and −10 mV, was 0.64 ± 0.06 ($n$ = 3). The mean value for $K_{d(0)}$ was 2.7 ± 0.2 mM ($n$ = 3). Given that putrescine has two positive charges, the average value for δ was 0.32 ± 0.03, which is identical to the corresponding value for spermine. Thus, spermine and putrescine share common or overlapping binding sites. The mean hill coefficient for putrescine was independent of voltage and displayed an average value near 0.8 (Fig. 8*D*).

## Discussion

This report demonstrates that naturally occurring polyamines induce strong inward rectification in the olfactory

CNG channel. Qualitatively similar effects of polyamines have previously been reported in a variety of channels, including $K_{ir}$ channels (Fakler et al., 1994; Ficker et al., 1994; Lopatin, Makhina & Nichols, 1994), glutamate receptor (GluR) channels (Bowie & Mayer, 1995; Donevan & Rogawski, 1995; Kamboj, Swanson & Cull-Candy, 1995), voltage-gated $Ca^{2+}$ and $K^+$ channels (Droiun & Hermann, 1994), $K_{ATP}$ channels (Niu & Meech, 1998), $Ca^{2+}$-activated $K^+$ channels (Weiger, Langer & Hermann, 1998), nicotinic acetylcholine receptor (nAchR) channels (Haghighi & Cooper, 1998), and most recently, for the retinal rod CNG $\alpha$ subunit (Lu & Ding, 1999). In some cases, a classical channel blocking mechanism can explain polyamine inhibition, but in others it appears that polyamines interact with the channel gating mechanism. The present study concludes that polyamines act at least partly via an allosteric inhibitory mechanism, and suggests that spermine could be an important physiological regulator of the olfactory CNG channel *in vivo.*

## Spermine Block at Negative Potentials

The model of ion channel block described by Woodhull (1973) assumes that charged blocking molecules bind to a single point site within the pore, where their dissociation rate constants are controlled by the membrane electrical field. In the simplest version of this model, the blocking molecule is assumed to be impermeant, that it acts *via* a single-step binding reaction and that it does not compete with the permeating ion for the binding site. As discussed in more detail below, it is probable that all of these assumptions are violated to some degree in the case of spermine block of the olfactory CNG channel. Nevertheless, this model does offer some useful insights into the mechanism of spermine inhibition. Over the voltage range from −120 to 0 mV, spermine induces a strongly voltage-dependent block, for which the Woodhull model predicts an average $z\delta$ of 1.27 + 0.13, and a $K_{d(0)}$ of 39 ± 7 μM. Assuming that all 4 of the positive charges on the spermine molecule contribute to the binding reaction, the $z\delta$ predicts a spermine binding site located at 32% of the electrical distance through the pore from the internal membrane surface.

An unexpected characteristic of instantaneous spermine block is that the maximal value of the Hill coefficient was significantly <1 (Fig. 3*F*). The most likely interpretation for this is that the spermine-induced inhibition results at least partly from a spermine-induced conformational change in the pore rather than by a direct blocking action. A similar mechanism was recently proposed to explain fast $Sr^{2+}$ inhibition of $Ca^{2+}$-activated $K^+$ channels (Sugihara, 1998). Another unusual finding was that the Hill coefficient for spermine inhibition increased significantly over the voltage range from −70 to −10 mV (Fig. 3*F*). This implies a voltage-dependence in the efficacy with which spermine interacts with the gating machinery, and thus, provides evidence for a voltage-dependent conformational change in the pore. Furthermore, in Fig. 5*C,* it is apparent that the concentration dependence of the rate of block saturates at the relatively low value of 200 $sec^{-1}$ at +120 mV. This behavior is not characteristic of a classical channel blocker (Hille, 1992) and thus provides further evidence for an allosteric inhibitory mechanism.

Polyamine inhibition of other channel types has also been explained in terms of both channel block and allosteric mechanisms. For example, polyamine inhibition of GluR6 glutamate receptor channels can be modelled mainly as channel block (Bähring et al., 1997), although they may also induce allosteric effects (Bähring & Mayer, 1998; Bowie, Lange & Mayer, 1998). A simple channel block mechanism appears to adequately account for the actions of polyamines on the $Ca^{2+}$-activated $K^+$ channels (Weiger et al., 1998) and nAchR channels (Haghighi & Cooper, 1998). On the other hand, polyamine effects on $K_{ATP}$ appear to be dominated by interactions with channel gating (Niu & Meech, 1998). Interestingly, polyamine inhibition of $K_{ir}2.1$ has been interpreted both as channel block (Lopatin et al., 1995; Lopatin & Nichols, 1996; Pearson & Nichols, 1998) and allosteric inhibition (Aleksandrov, Velimirovic & Clapham, 1996). Polyamines can also act as excitatory modulatory agents in NMDA receptors (Benveniste & Mayer, 1993) and nAchRs (Shao et al., 1998).

## Spermine Permeation and Block at Positive Potentials

In the presence of spermine, the CNG channel peak conductance reached a local minimum near 0 mV. At voltages greater than 0 mV, the peak conductance increased slightly (Fig. 2*A*). This increase is most likely due to spermine permeation through the channel. Spermine, which has a minimum cross-sectional area of about 16 $Å^2$ (Bähring et al., 1997), has previously been shown to permeate GluR6 (Bähring et al., 1997) and nAchR channels (Haghighi & Cooper, 1998), but not $K_{ir}2.1$ (e.g., Lopatin et al., 1995). Molecular sieving experiments have revealed that both the GluR and the nAchR have effective pore cross-sectional areas of 40.3 and 44.2 $Å^2$, respectively (Burnashev, Villarroel & Sakmann, 1996; Dwyer, Adams & Hille, 1980). Such a pore magnitude is easily sufficient to permit the passage of a molecule the size of spermine. On the other hand, the pore cross-section of $K^+$ channels is 8.6 $Å^2$ (Hille, 1973), which is too small to allow spermine permeation. Since the olfactory channel has a cross-section of at least 42 $Å^2$ (Balasubramanian, Lynch & Barry, 1995), spermine is indeed expected to be permeable. However, part of the

peak channel conductance at positive potentials may be due to incomplete block. That is, the channel may still conduct $Na^+$ even though the spermine instantaneous binding sites are saturated. Such an effect of spermine has previously been reported in GluR6 (Bähring et al., 1997) and in $K_{ir}4.1$ (Oliver et al., 1998).

In addition to the instantaneous block seen at negative membrane potentials, step depolarizations to positive voltages induced an exponential current decay to a steady-state blocked level (Fig. 1*A*). At high enough spermine concentrations and voltages, this block is essentially complete (Fig. 2*B*). Woodhull modeling applied to steady-state block revealed a $z\delta$ of 1.18 ± 0.06 and a $K_{d(0)}$ of 2.6 ± 0.7 mM. This $z\delta$ value is not significantly different to that of the instantaneous block observed at negative potentials, although the $K_{d(0)}$ is 67 times higher. The similarity in the $z\delta$ values constitutes strong evidence that both instantaneous and steady-state block is mediated by adjacent spermine binding sites. Given this finding, it is relevant to consider why a much higher driving force is required for steady-state block than for instantaneous block. Since steady-state block and instantaneous block occur simultaneously at positive membrane potentials, a single common binding site with a voltage-dependent binding affinity can be ruled out. However, one plausible possibility is that there are two identical spermine sites located at a similar depth in the pore. Occupation of the first site occurs rapidly and with relatively high affinity, but once a spermine molecule has bound, it inhibits spermine occupation of the second binding site via electrostatic repulsion. This repulsion is overcome at higher membrane potentials, but results in a lower apparent binding affinity for the second spermine molecule. The pore permits residual $Na^+$ flux when a single spermine molecule is bound, but the binding of a second molecule effectively blocks all ionic flux. An attractive feature of this model is that it is consistent with the recently proposed dimeric pore structure for CNG channels (Liu et al., 1998). Mutual electrostatic repulsion by spermine molecules in the pore has previously been invoked by Lopatin et al. (1995, 1996) to model spermine block of $K_{ir}2.1$. However, in this later model, the molecules were located end-to-end rather than side-by-side.

Polyamine block of the recombinantly expressed rod CNG channel α subunit was recently investigated by Lu and Ding (1999) and published after completion of this study. Although their use of a relatively slow (25–50 $mV/sec^{-1}$) voltage-ramp protocol would have obscured the existence of an instantaneous spermine inhibitory component, the complex shape of the steady-state inhibition curves was generally similar to that observed here. Based on analysis of these curves, Lu and Ding concluded that spermine could block the pore in either a linear (permeant) or curled (nonpermeant) conformation. However, such a mechanism cannot explain the results of the present study, as the nonpermeant blocked conformation requires the binding of two discrete molecules at a similar depth in the pore. The characterisitcs of polyamine inhibition also differed in other respects. For example, at negative potentials the spermine blocking affinity for the rod channel was about 6 times more sensitive than for the olfactory channel, although the spermidine and purescine affinities were comparable. There also appeared to be significant differences in the voltage-dependence of spermine permeation and inhibition. Finally, Lu and Ding found no evidence for an allosteric mechanism of spermine inhibition.

### Permeation and Inhibition by Spermidine and Putrescine

The inhibitory actions of spermidine and putrescine were also investigated. Woodhull analysis of spermidine block predicts an average value for $z\delta$ of 1.13 ± 0.06 ($n = 5$) and for $K_{d(0)}$ of 121 ± 16 ($n = 5$). Given that $z = +3$, this yields a mean δ of 0.38 ± 0.02, which was not significantly different to the corresponding value for spermine inhibition. Putrescine block is characterized by an average $z\delta$ of 0.64 ± 0.06 ($n = 3$) and a $K_{d(0)}$ of 2.7 ± 0.2 mM ($n = 3$). Since putrescine has 2 positive charges, this yields a mean value for δ of 0.32 ± 0.02. This is identical to the corresponding value for spermine steady-state block, indicating that putrescine, spermidine and spermine share common or overlapping binding sites. Since spermidine and putrescine display no time-dependent component of block (Figs. 7*A* and 8*A*), it is not possible to compare their mode of action with that of spermine. However, the lack of spermidine- and putrescine-induced relaxations is generally consistent with their lower affinity, suggesting that their kinetics of block and unblock are much faster than those of spermine. Hence, during voltage steps, equilibrium is reached much faster for spermidine and putrescine than for equivalent concentrations of spermine. The mean Hill coefficient for spermidine and putrescine binding are both <1, but display no significant voltage-dependence (Fig. 7*D* and 8*D*). Thus, both spermidine and putrescine also appear to act at least partially via allosteric inhibitory mechanisms.

### Physiological Relevance

The endogenous polyamines, spermine, spermidine and putrescine, are present in virtually all cell types. They are absolutely required for protein synthesis, cell division and cell growth in both normal and neoplastic cells (reviewed in Tabor & Tabor, 1984). It might therefore be expected that they would be particularly important in olfactory receptor neurons, which regenerate continually

throughout life. However, to date there has been no investigation into the role of polyamines in the differentiation, growth or mature physiological functioning of olfactory receptor neurons. Intracellular polyamines typically exist at total concentrations in the millimolar range (Ortiz, Giacobini & Schmidt-Glenewinkel, 1983), but are usually strongly buffered so that free concentrations are at least an order of magnitude lower (Tabor & Tabor, 1984). For example, one study predicted a total internal spermine concentration in the range 0.88–1.57 mM, with a free concentration in the range 8–76 μM (Watanabe et al., 1991). In agreement with these later figures, patch-clamp analyses of polyamine-induced ion channel rectification in intact cells have predicted intracellular free spermine concentrations around 50 μM (Bowie & Mayer, 1995; Haghighi & Cooper, 1998). Therefore, since spermine inhibits the olfactory CNG channel with a $K_{d(0)}$ of 39 μM, it is likely to exert a strong voltage-dependent channel block at physiological concentrations. However, the spermine-induced inward rectification of olfactory CNG channels may not be readily apparent in odorant-mediated currents because these are comprised of both cation current influx through CNG channels and $Cl^-$ efflux through $Ca^{2+}$-activated $Cl^-$ channels (Kurahashi & Yau, 1993; Lowe & Gold, 1993). Nevertheless, spermine-induced block of CNG channels is likely to significantly reduce the whole-cell conductance over the voltage range between −50 and −20 mV. This could have important consequences for neuronal excitability around the action potential threshold and for $Ca^{2+}$ entry during the odorant response.

I gratefully acknowledge the support of the National Health and Medical Research Council of Australia and the Garnett Passe and Rodney Williams Memorial Foundation.

## References

Aleksandrov, A., Velimirovic, B., Clapham, D.E. 1996. Inward rectification of the IRK1 $K^+$ channel reconstituted in lipid bilayers. *Biophys. J.* **70:**2680–2687

Bähring, R., Bowie, D., Benveniste, M., Mayer, M.L. 1997. Permeation and block of rat GluR6 glutamate receptor channels by internal and external polyamines. *J. Physiol.* **502:**575–589

Bähring, R., Mayer, M.L. 1998. An analysis of philanthotoxin block for recombinant rat GluR6(Q) glutamate receptor channels. *J. Physiol.* **509:**635–650

Balasubramanian, S., Lynch, J.W., Barry, P.H. 1995. The permeation of organic cations through cAMP-gated channels in mammalian olfactory receptor neurons. *J. Membrane Biol.* **146:**177–191

Benveniste, M., Mayer, M.L. 1993. Multiple effects of spermine on N-methyl-D-aspartic acid receptor responses of rat cultured hippocampal neurones. *J. Physiol.* **464:**131–63

Bowie, D., Lange, G.D., Mayer, M.L. 1998. Activity-dependent modulation of glutamate receptors by polyamines. *J. Neurosci.* **18:**8175–8185

Bowie, D., Mayer, M.L. 1995. Inward rectification of both AMPA and kainate subtype glutamate receptors generated by polyamine-mediated ion channel block. *Neuron* **15:**453–462

Burnashev, N., Villarroel, A., Sakmann, B. 1996. Dimensions and ionic selectivity of recombinant AMPA and kainate receptor channels and their dependence on Q/R site residues. *J. Physiol.* **496:**165–173

Colquhoun, D., Farrant, M. 1993. The binding issue. *Nature* **366:**510–511

Donevan, S.D., Rogawski, M.A. 1995. Intracellular polyamines mediate inward rectification of $Ca^{2+}$-permeable a-amino-3-hydroxy-5-methyl-4-isoxazoleproprionic acid receptors. *Proc. Natl. Acad. Sci. USA* **92:**9298–9302

Drouin, H., Hermann, A. 1994. Intracellular action of spermine on neuronal $Ca^{2+}$ and $K^+$ currents. *Eur. J. Neurosci.* **6:**412–419

Dwyer, T.M., Adams, D.J., Hille, B. 1980. The permeability of the endplate channel to organic cations in frog muscle. *J. Gen. Physiol.* **75:**469–492

Fakler, B., Brandle, U., Glowatzski, E., Konig, C., Bond, C., Adelman, J.P., Zenner, H.-P., Ruppersburg, J.P. 1994. S structural determinant of the differential sensitivity of cloned inward-rectifier $K^+$ channels to intracellular spermine. *FEBS Lett.* **356:**199–203

Fakler, B., Brandle, U., Glowatzski, E., Weidemann, S., Zenner, H.-P., Ruppersberg, J.P. 1995. Strong voltage-dependent inward rectification of inward rectifier $K^+$ channels is caused by intracellular spermine. *Cell* **80:**149–154

Ficker, E., Taglialatela, M., Wible, B.A., Henley, C.M., Brown, A.M. 1994. Spermine and spermidine as gating molecules for inward rectifier $K^+$ channels. *Science* **266:**1068–1072

Frings, S., Lynch, J.W., Lindemann, B. 1992. Properties of cyclic nucleotide-gated channels mediating olfactory transduction: activation, selectivity, and blockage. *J. Gen. Physiol.* **100:**45–67

Frings, S., Seifert, R., Godde, M., Kaupp, U.B. 1995. Profoundly different calcium permeation and blockage determine the specific function of distinct cyclic nucleotide-gated channels. *Neuron* **15:**169–179

Haghighi, A.P., Cooper, E. 1998. Neuronal nicotinic acetylcholine receptors are blocked by intracellular spermine in a voltage-dependent manner. *J. Neurosci.* **18:**4050–4062

Hille, B. 1973. Potassium channels in myelinated nerve: selective permeability to small cations. *J. Gen. Physiol.* **61:**669–686

Hille, B. 1992. Ionic channels of excitable membranes. 2nd ed. Sinauer Associates, Sunderland, MA

Kamboj, S.K., Swanson, G.T., Cull-Candy, S. G. 1995. Intracellular spermine confers rectification on rat calcium-permeable AMPA and kainate receptors. *J. Physiol.* **486:**297–303

Kurahashi, T., Shibuya, K. 1990. $Ca^{2+}$-dependent adaptive properties in the solitary olfactory receptor of the newt. *Brain Res.* **515:**261–268

Kurahashi, T., Yau, K.W. 1993. Co-existence of cationic and anionic components in odorant-induced current of vertebrate olfactory receptor cells. *Nature* **363:**71–74

Lopatin, A.N., Makhina, E.N., Nichols, C.G. 1994. Potassium channel block by cytoplasmic polyamines as the mechanism of intrinsic rectification. *Nature* **372:**366–369

Lopatin, A.N., Makhina, E.N., Nichols, C.G. 1995. The mechanism of inward rectification of potassium channels: "long-pore plugging" by cytoplasmic polyamines. *J. Gen. Physiol.* **106:**923–955

Lopatin, A.N., Nichols, C.G. 1996. [$K^+$] dependence of polyamine-induced rectification in inward rectifier potassium channels (IRK1, Kir2.1). *J. Gen. Physiol.* **108:**105–113

Lowe, G., Gold, G.H. 1993. Nonlinear amplification by calcium-dependent chloride channels in olfactory receptor cells. *Nature* **366:**283–285

Liu, D.T., Tibbs, G.R., Paoletti, P., Siegelbaum, S.A. 1998. Constraining ligand-binding site stoichiometry suggests that a cyclic nucleo-

tide-gated channel is composed of two functional dimers. *Neuron* **21:**235–248

Lu, Z., Ding, L. 1999. Blockade of a retinal cGMP-gated channel by polyamines. *J. Gen. Physiol.* **113:**35–43

Lynch, J.W., Barry, P.H. 1991. Properties of transient $K^+$ current and underlying single $K^+$ channels in rat olfactory receptor neurons. *J. Gen. Physiol.* **97:**1043–1072

Lynch, J.W., Lindemann, B. 1994. Cyclic nucleotide-gated channels of rat olfactory receptor neurons: divalent cations control the sensitivity to cAMP. *J. Gen. Physiol.* **103:**87–106

Nichols, C.G., Lopatin, A.N. 1997. Inward rectifier potassium channels. *Annu. Rev. Physiol.* **59:**171–191

Niu, X.W., Meech, R.W. 1998. The effect of polyamines on $K_{ATP}$ channels in guinea-pig ventricular myocytes. *J. Physiol.* **508:**401–411

Oliver, D., Hahn, H., Antz, C., Ruppersberg, J.P., Fakler, B. 1998. Interaction of permeant and blocking ions in cloned inward-rectifier $K^+$ channels. *Biophys. J.* **74:**2318–2326

Ortiz, J.G., Giacobini, E., Schnmidt-Glenewinkel, T. 1983. Acetylation of polyamines in mouse brain: subcellular and regional distribution. *J. Neurosci. Res.* **9:**193–201

Pearson, W.L., Nichols, C.G. 1998. Block of the Kir2.1 channel pore by alkylamine analogues of endogenous polyamines. *J. Gen. Physiol.* **112:**351–363

Shao, Z., Mellor, I.R., Brierley, M.J., Harris, J., Usherwood, P.N.R. 1998. Potentiation and inhibition of nicotinic acetylcholine receptors by spermine in the TE671 human muscle cell line. *J. Pharmacol. Exp. Ther.* **286:**1269–1276

Sugihara, I. 1998. Activation and two modes of blockade by strontium of $Ca^{2+}$-activated $K^+$ channels in goldfish saccular cells. *J. Gen. Physiol.* **111:**363–379

Tabor, C.W., Tabor, H. 1984. Polyamines. *Annu. Rev. Biochem.* **53:**749–790

Watanabe, S.-I., Kusama-Eguchi, K., Kobayashi, H., Igarashi, K. 1991. Estimation of polyamine binding to macromolecules and ATP in bovine lymphocytes and rat liver. *J. Biol. Chem.* **266:**20803–20809

Weiger, T.M., Langer, T., Hermann, A. 1998. External action of di- and polyamines on maxi calcium-activated potassium channels: an electrophysiological and molecular modeling study. *Biophys. J.* **74:**722–730

Williams, K. 1997. Interactions of polyamines with ion channels. *Biochem. J.* **325:**289–297

Woodhull, A. 1973. Ionic blockage of sodium channels in nerve. *J. Gen. Physiol.* **61:**687–708

Zufall, F., Firestein, S. 1993. Divalent cations block the cyclic nucleotide-gated channel of olfactory receptor neurons. *J. Neurophysiol.* **69:**1758–1768